System-level Performance of Interference Alignment

Ratheesh K. Mungara, *Student Member, IEEE*, David Morales-Jimenez, *Member, IEEE*, and Angel Lozano, *Fellow, IEEE*

***Abstract*—Capitalizing on the analytical potency of stochastic geometry and on some new ideas to model intercell interference, this paper presents analytical expressions that enable quantifying the spectral efficiency of IA (interference alignment) in cellular networks without the need for simulation. From these expressions, the benefits of IA are characterized. Even under favorable assumptions, IA is found to be beneficial only in very specific and relatively infrequent network situations, and a blanket utilization of IA is found to be altogether detrimental. Applied only in the appropriate situations, IA does bring about benefits that are significant for the users involved but relatively small in terms of average spectral efficiency for the entire system.**

***Index Terms*—Interference alignment, stochastic geometry, Poisson point process, spatial multiplexing, spectral efficiency, distributed cooperation.**

I. Introduction

The mitigation of intercell interference has been, for quite some time, one of the main thrusts in wireless communications research. Of late, BS (base station) cooperation has gained the perception of being the best way to counter intercell interference. Among the various cooperation schemes being considered stands IA (interference alignment), which has the advantage of admitting distributed implementations [2], [3]. At the expense of instantaneous CSI (channel state information) at both transmitters and receivers, IA ensures that the interference from all participating users aligns at each receiver along a certain subspace leaving the remaining dimensions free of interference [4], [5]. In toy settings where all the users can participate in the alignment and the CSI is perfect, IA can deliver an unbounded growth of the spectral efficiency with the SNR (signal-to-noise ratio).

The favorable IA behavior encountered in small toy settings, however, does not extrapolate to larger wireless networks. Depending on the antenna counts, only a limited number of users can participate in the alignment; with two antennas, for instance, at most three users can participate. This necessarily leads to the formation of relatively small IA clusters that are inevitably exposed to interference from all other users in the system. Thus, even the subspaces that IA protects from in-cluster interference are bound to experience out-of-cluster interference [6]. In addition, IA restricts the spatial dimensionality of the transmit signals; in the two-antenna three-user example, the spatial dimensionality of the signals cannot exceed one; without IA, in contrast, a two-dimensional signal could be transmitted applying standard SU-MIMO (single-user multiple-input multiple-output) techniques. Altogether then, IA can create subspaces with reduced interference in exchange for a sacrifice in signal dimensions. Naturally, the question arises of whether and when this tradeoff is justified in the context of modern wireless networks. This question is precisely what motivates this paper.

In contrast with some prior works on the system-level performance of IA, which relied on simulations over grid networks [7]–[10], we set out to address the matter analytically in order to attain broader generality and more pronounced guidance in the conclusions. This naturally leads us to invoke the tools of stochastic geometry, which allow for models that (*i*) are more amenable to analytical treatment, and (*ii*) are arguably more representative of the heterogeneous structure of emerging wireless networks [11]–[17]. We utilize PPP (Poisson Point Process) distributions to model the locations of BSs and users, yet the methodology could be equally applied with more sophisticated spatial distributions [18], [19].

In order to address the afore-posed question of whether and when the dimensionality sacrifice entailed by IA is advantageous, we posit SU-MIMO as a baseline for interference-oblivious techniques that utilize all available dimensions for signalling. SU-MIMO is a conservative baseline in the sense that it has less stringent requirements than IA in every respect, chiefly in terms of CSI. Then, for given antenna counts and relevant propagation conditions, we seek to compare the system-level spectral efficiencies achievable reliably with IA and with SU-MIMO. In order to keep the comparison indeed conservative, assumptions that are highly favorable to IA are made throughout. Specifically:

- Perfect transmit and receive CSI is assumed, with all the corresponding overheads neglected.
- Instantaneous availability of the optimum IA precoders is also assumed, neglecting the iterative processes that might be required to actually compute such precoders.
- The clusters of BSs effecting IA are determined dynamically, with user locations and propagation conditions taken into account. This improves the performance of IA relative to static clusters defined a-priori [9], [17], [20].
- Interference-limited conditions are considered, with thermal noise neglected. Everything else being the same, this maximizes the benefits of IA.

The analysis is conducted for the downlink, which is the link that seems more apt to accommodate IA. Borrowing techniques from [21], [22], the analysis could be extended to incorporate directional antennas and sectorization; while

R. K. Mungara and A. Lozano are with the Department of Information and Communication Technologies, Universitat Pompeu Fabra (UPF), 08018 Barcelona, Spain. E-mail: {ratheesh.mungara, angel.lozano}@upf.edu.

D. Morales-Jimenez was with Universitat Pompeu Fabra. He is now with the Department of Electronic and Computer Engineering, Hong Kong University of Science and Technology, Clear Water Bay, Kowloon, Hong Kong. Email: eedmorales@ust.hk.

This work was supported by the European Project FET 265578 "HIATUS". This paper is accepted for presentation in parts at the 2014 IEEE Global Communications Conference (GLOBECOM) [1].

quantitatively very interesting, this extension is not expected to modify the qualitative conclusions.

II. System Model

Consider a cellular network with BSs located according to a homogeneous PPP $\Phi_{\rm b} \subset \mathbb{R}^2$ with density $\lambda_{\rm b}$. The user locations are modeled by another independent PPP $\Phi_{\rm u}$ with density $\lambda_{\rm u}$. The BSs and users are respectively equipped with $N_{\rm t}$ transmit and $N_{\rm r}$ receive antennas, and each link carries $d \leq \min(N_{\rm t}, N_{\rm r})$ signal streams. We denote by P the fixed power transmitted by each BS. Without loss of generality, we consider a user located at the origin to conduct the analysis.

Given the prevalence of log-normal shadowing in terrestrial wireless systems, the shadowing between any BS and the user is represented by $\mathcal{X} \sim 10^{\mathcal{N}_{\mathbb{C}}(0,\sigma^2_{\rm dB})/10}$ where $\mathcal{N}_{\mathbb{C}}(0,\sigma^2_{\rm dB})$ is a zero-mean complex Gaussian random variable with variance $\sigma^2_{\rm dB}$. With shadowing, the strongest BS need not necessarily be the closest one and the average power received by the user from any BS is a function of the distance-dependent pathloss as well as the shadowing of the corresponding link. And, provided that $\mathbb{E}[\mathcal{X}^{2/\eta}] < \infty$ (with $\eta > 2$ the pathloss exponent), the distribution of average powers received at the user from all the BSs is identical to the distribution of the powers received from BSs populated according to a different homogeneous PPP $\Phi_{\mathsf{r}} \subset \mathbb{R}^2$ with density [23, Theorem 2]

$$\lambda_{\mathsf{r}} = \lambda_{\rm b}\, \mathbb{E}\left[\mathcal{X}^{2/\eta}\right] \tag{1}$$

and with the same transmit power P, but without shadowing on the links. Therefore, the BS density λ_{r} captures the effect of shadowing and the subsequent analysis is conducted using the equivalent PPP Φ_{r}.

A set of BSs jointly performing IA are collectively referred to as a cluster. Denote by r_k the distance between the user at the origin and the kth BS (whose location is distributed according to Φ_{r}, capturing the effect of shadowing). Without loss of generality, we index the BSs in increasing order of r_k, i.e., $\mathsf{r}_k < \mathsf{r}_{k+1}\ \forall k$. We consider dynamic clustering, where the K BSs with the strongest links or, equivalently, the smallest distances, $\{\mathsf{r}_0, \ldots, \mathsf{r}_{K-1}\}$, compose the IA cluster. The first of them ($k = 0$) acts as the serving BS.

In light of the foregoing considerations, the observation $\boldsymbol{y} \in \mathbb{C}^{N_{\rm r}\times 1}$ at the user can be written as

$$\boldsymbol{y} = \sqrt{\frac{P}{d}} \sum_{k=0}^{K-1} \mathsf{r}_k^{-\eta/2} \boldsymbol{H}_k \boldsymbol{x}_k + \boldsymbol{z}' \tag{2}$$

where the leading term contains the in-cluster signals while

$$\boldsymbol{z}' = \sqrt{\frac{P}{d}} \sum_{k=K}^{\infty} \mathsf{r}_k^{-\eta/2} \boldsymbol{H}_k \boldsymbol{x}_k \tag{3}$$

represents the out-of-cluster interference. In turn, $\boldsymbol{x}_k \in \mathbb{C}^{N_{\rm t}\times 1}$ is the signal transmitted by the kth BS, and $\boldsymbol{H}_k \in \mathbb{C}^{N_{\rm r}\times N_{\rm t}}$ is the fading matrix between the kth BS and the user, perfectly known at both ends. The entries of $\boldsymbol{H}_k$ are independent identically distributed (IID) samples drawn from $\mathcal{N}_{\mathbb{C}}(0,1)$. The signal transmitted by the kth BS is $\boldsymbol{x}_k = \boldsymbol{V}_k \boldsymbol{b}_k$ where $\boldsymbol{V}_k = [\boldsymbol{v}_{k,1} \cdots \boldsymbol{v}_{k,d}] \in \mathbb{C}^{N_{\rm t}\times d}$ is a unitary precoder (meaning a matrix whose columns are orthonormal) and $\boldsymbol{b}_k \in \mathbb{C}^{d\times 1}$ is a vector of IID complex Gaussian symbols satisfying $\mathbb{E}[\boldsymbol{b}_k \boldsymbol{b}_k^*] = \boldsymbol{I}_d$. With that, the power is uniformly allocated across the d signal streams and $\mathbb{E}[\|\boldsymbol{x}_k\|^2] = d$. At the receiver, the kth user applies a unitary filter $\boldsymbol{W}_k$.

III. Interference Alignment

With perfect CSI, IA yields a d-dimensional channel free of in-cluster interference for every link [4]. If $\min(N_{\rm t}, N_{\rm r}) \geq 2d$, then a necessary and sufficient condition for IA feasibility is [24]

$$N_{\rm t} + N_{\rm r} \geq (K+1)\, d. \tag{4}$$

The precoders $\boldsymbol{V}_0, \ldots, \boldsymbol{V}_{K-1}$ and the receive filter $\boldsymbol{W}_0$ that effect IA satisfy

$$\operatorname{rank}(\boldsymbol{W}_0^* \boldsymbol{H}_0 \boldsymbol{V}_0) = d \tag{5}$$

$$\boldsymbol{W}_0^* \boldsymbol{H}_k \boldsymbol{V}_k = \boldsymbol{0} \qquad k \neq 0 \tag{6}$$

as well as similar conditions for the other $K-1$ users being served concurrently in the same cluster. After applying the filter $\boldsymbol{W}_0 = [\boldsymbol{w}_{0,1}, \ldots, \boldsymbol{w}_{0,d}] \in \mathbb{C}^{N_{\rm r}\times d}$, the receiver at the origin observes

$$\boldsymbol{W}_0^* \boldsymbol{y} = \sqrt{\frac{P}{d}} \mathsf{r}_0^{-\eta/2} \boldsymbol{W}_0^* \boldsymbol{H}_0 \boldsymbol{V}_0 \boldsymbol{b}_0 + \boldsymbol{W}_0^* \boldsymbol{z}' \tag{7}$$

where, by virtue of (6), there is no interference contribution from the in-cluster BSs.

Throughout this paper, the precoders and receive filters are obtained through the Min-Leakage algorithm [2] with the overheads associated with running this algorithm neglected.

IV. Out-of-Cluster Interference Modelling

An instrumental step in our analysis is the modelling of the out-of-cluster interference $\boldsymbol{z}'$, which in interference-limited conditions is the remaining obstacle to reliable communication. As can be gauged from (3), $\boldsymbol{z}'$ involves a linear combination of terms involving products of Gaussian variates, altogether difficult to manipulate and conduct analysis with. Albeit certain characterizations of its exact distribution are plausible (cf. [17], [25]–[28]), in this paper we take an alternative path that promises a better payoff in terms of analytical insight. Recognizing that $\boldsymbol{z}'$ consists of a large number of independent terms whose fading is unknown by the user of interest, we replace it by a zero-mean complex Gaussian random vector with matching covariance $\mathbb{E}[\boldsymbol{z}'\boldsymbol{z}'^*]$. This model, whose goodness is validated later in the paper, turns out to be highly precise. And, besides the central limit theorem, there are information-theoretic arguments in favor of modeling the out-of-cluster interference as complex Gaussian with a power dictated by the locations of the interferers:

- If the exact distribution of the out-of-cluster interference is either unknown or ignored by the receiver, with a codebook and decoder designed to handle Gaussian noise, then the achievable spectral efficiency is precisely as if the interference were indeed Gaussian [29]. Thus, the spectral efficiencies in this paper can be interpreted as

those achievable with standard Gaussian-noise signaling and decoding.

- For a given interference covariance, complex Gaussian is the worst possible interference distribution in terms of the spectral efficiency achievable with complex Gaussian signaling. Hence, the spectral efficiencies in this paper can also be interpreted as lower bounds (quite tight judging from Example 2) to the spectral efficiency with optimum signaling and decoding.

From (3), the conditional covariance of $\boldsymbol{z}'$ for given interferer locations, which—recall—incorporate the effect of the corresponding shadowings, is

$$\mathbb{E}\left[\boldsymbol{z}'\boldsymbol{z}'^{*}\,|\,\{\mathsf{r}_k\}\right] = \frac{P}{d}\sum_{k=K}^{\infty}\mathsf{r}_k^{-\eta}\,\mathbb{E}\left[\boldsymbol{H}_k\boldsymbol{x}_k\boldsymbol{x}_k^{*}\boldsymbol{H}_k^{*}\right] \tag{8}$$

$$= \frac{P}{d}\sum_{k=K}^{\infty}\mathsf{r}_k^{-\eta}\,\mathbb{E}\left[(\boldsymbol{H}_k\boldsymbol{V}_k)(\boldsymbol{H}_k\boldsymbol{V}_k)^{*}\right] \tag{9}$$

$$= P\sum_{k=K}^{\infty}\mathsf{r}_k^{-\eta}\boldsymbol{I}_{N_{\mathrm{r}}} \tag{10}$$

where (8) follows from the mutual independence of $\{\boldsymbol{x}_k\}_{k=K}^{\infty}$ while (10) follows from the fact that $(\boldsymbol{H}_k\boldsymbol{V}_k)$ is an $N_{\mathrm{r}}\times d$ matrix with IID zero-mean unit-variance entries such that $\mathbb{E}\left[(\boldsymbol{H}_k\boldsymbol{V}_k)(\boldsymbol{H}_k\boldsymbol{V}_k)^{*}\right] = d\,\boldsymbol{I}_{N_{\mathrm{r}}}$.

Since the locations and shadowings of the interferers are themselves random, we can take a further expectation over those quantities with the hope that the ensuing unconditioned interference covariance be representative of most instances thereof. Again, the goodness of this step is validated later. Then, $\mathbb{E}[\boldsymbol{z}'\boldsymbol{z}'^{*}] = P\sigma_0^2\boldsymbol{I}_{N_{\mathrm{r}}}$ with

$$\sigma_0^2 = \mathbb{E}_{\Phi_{\mathsf{r}}}\left[\sum_{k=K}^{\infty}\mathsf{r}_k^{-\eta}\right] \tag{11}$$

and the potency of the stochastic modelling approach is shown in full force by the fact that this expectation can be computed explicitly, yielding (cf. Appendix A)

$$\sigma_0^2 = \frac{2\pi\lambda_{\mathsf{r}}}{\eta-2}\mathsf{r}_{K-1}^{2-\eta}. \tag{12}$$

With the out-of-cluster interference thus modeled, and recalling the desired signal term in (7), the instantaneous SIR (signal-to-interference ratio) experienced by the ℓth signal stream is

$$\mathrm{SIR}_\ell = \frac{\frac{P}{d}\mathsf{r}_0^{-\eta}\,\mathbb{E}\left[|[\boldsymbol{W}_0^{*}\boldsymbol{H}_0\boldsymbol{V}_0\boldsymbol{b}_0]_\ell|^2\,|\,\{\boldsymbol{H}_k\}\right]}{P\sigma_0^2} \tag{13}$$

where $[\cdot]_\ell$ indicates the ℓth entry of a vector and the expectation in the numerator is over $\boldsymbol{b}_0$, conditioned on the fading (and therefore on the precoders and receivers). Evaluating such expectation,

$$\mathrm{SIR}_\ell = \frac{\frac{P}{d}\mathsf{r}_0^{-\eta}|\boldsymbol{w}_{0,\ell}^{*}\boldsymbol{H}_0\boldsymbol{v}_{0,\ell}|^2}{P\sigma_0^2} \tag{14}$$

$$= \frac{\rho^{\mathsf{IA}}|\boldsymbol{w}_{0,\ell}^{*}\boldsymbol{H}_0\boldsymbol{v}_{0,\ell}|^2}{d} \tag{15}$$

where

$$\rho^{\mathsf{IA}} = \frac{\mathsf{r}_0^{-\eta}}{\sigma_0^2} \tag{16}$$

$$= \frac{\mathsf{r}_{K-1}^{\eta-2}}{\mathsf{r}_0^{\eta}}\frac{\eta-2}{2\pi\lambda_{\mathsf{r}}} \tag{17}$$

is the local-average SIR at the user of interest.

Note that $\{\mathrm{SIR}_\ell\}_{\ell=1}^{d}$ are mutually dependent, through $\boldsymbol{H}_0$, but identically distributed and hence to characterize the marginal distribution of the per-stream SIR we can drop the stream index ℓ. Such characterization is the object of Section V, as a stepping stone towards the evaluation of the spectral efficiency in Section VI. Receivers whose performance depends on the joint distribution of the SIRs of all d streams are tackled directly in Section VI.

V. SIR Distribution

In this section we provide three different characterizations of the marginal per-stream SIR distribution, each accompanied by a corresponding interpretation. We begin with the most informative one, and then proceed onto more marginalized forms thereof.

A. Specific Absolute Cluster Geometry

For given locations (and shadowings), i.e., for given $\mathsf{r}_0,\ldots,\mathsf{r}_{K-1}$, the value of ρ^{IA} becomes determined. Since $\boldsymbol{v}_{0,\ell}$ and $\boldsymbol{w}_{0,\ell}$ are columns of matrices that are unitary and independent of $\boldsymbol{H}_0$, the effective instantaneous gain $|\boldsymbol{w}_{0,\ell}^{*}\boldsymbol{H}_0\boldsymbol{v}_{0,\ell}|^2$ for any stream ℓ is exponentially distributed with unit mean [2]. It follows from (17) that the instantaneous per-stream SIR exhibits Rayleigh fading with local-average ρ^{IA}/d and hence its conditional CDF (cumulative distribution function) is

$$F_{\mathrm{SIR}|\rho^{\mathsf{IA}}}(\gamma) = 1 - e^{-\gamma d/\rho^{\mathsf{IA}}}. \tag{18}$$

Through ρ^{IA}, the above distribution depends on the distance to the serving BS, r_0, and on the distance delimiting the IA cluster, r_{K-1}, and it can be utilized to establish the performance of IA as a function of these two key quantities. In contrast, the location of the other in-cluster BSs, $\mathsf{r}_1,\ldots,\mathsf{r}_{K-2}$, is immaterial because, by virtue of IA, they do not contribute any interference.

B. Specific Relative Cluster Geometry

Let us now marginalize the instantaneous SIR over r_0 and r_{K-1} while keeping their ratio $a_0 = \mathsf{r}_0/\mathsf{r}_{K-1}$ fixed. Note that $0 < a_0 < 1$ with probability 1.

Proposition 1. *For a given* $a_0 = \mathsf{r}_0/\mathsf{r}_{K-1}$,

$$F_{\mathrm{SIR}|a_0}(\gamma) = 1 - \left(1 + \frac{2\,a_0^{\eta}\,d}{\eta-2}\,\gamma\right)^{-K}. \tag{19}$$

Proof: See Appendix B. ∎

In contrast with (18), which—through ρ^{IA}—depends on the BS density λ_{b}, the CDF in Prop. 1 no longer depends on λ_{b}. In this distribution, the geometry of the cluster is captured

by a single parameter, a_0, which informs of the location of the serving BS relative to the edge of the IA cluster and thus relative to the out-of-cluster interferers. Put differently, a_0 informs in a compact fashion of where the user of interest is within the cluster: values close to 0 map to situations where the user is in the inner part of the cluster while values close to 1 map to situations where the user is in the periphery thereof. As will be seen, this characterization, conveniently scale independent, is highly indicative of IA performance. And, as one would anticipate, a_0 is also tightly related to the marginalized local-average per-stream SIR, something that can be verified by applying (19) to compute

$$\int_0^\infty \gamma \, \mathrm{d}F_{\mathrm{SIR}|a_0}(\gamma) = \frac{\eta - 2}{2a_0^\eta \, d \, (K-1)} \tag{20}$$

which must be interpreted with care because a_0 and K are not independent: its presence in the denominator notwithstanding, a larger K increases (20) because, everything else being the same, it results in a smaller a_0 and such contraction is magnified by the pathloss exponent η ultimately shrinking the denominator.[1] A proper interpretation of the marginalized distribution in Prop. 1 is of the utmost importance. It does not correspond to the distribution of the SIR experience by any actual user in the system, but rather it is a stepping stone towards the computation of other quantities later in the paper.

At this point, we validate $F_{\mathrm{SIR}|a_0}(\cdot)$ by contrasting it with its counterpart, obtained numerically, where $\boldsymbol{z}'$ is as in (3).

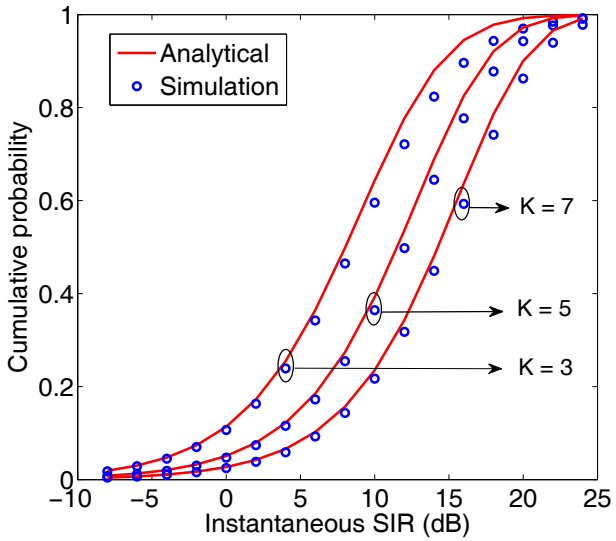

Fig. 1. CDF of the marginalized instantaneous per-stream SIR for IA with $d = 1$ and $\eta = 4$. Analytical and simulation results for $K = 3$ and $a_0 = 0.45$, for $K = 5$ and $a_0 = 0.32$, and for $K = 7$ and $a_0 = 0.25$.

Example 1. *Shown in Fig. 1 is a comparison of $F_{\mathrm{SIR}|a_0}(\cdot)$ with the simulated CDF of the corresponding SIR with $\boldsymbol{z}'$ as in (3). The comparison is conducted for $K = 3$ and $a_0 = 0.45$, for $K = 5$ and $a_0 = 0.32$, and for $K = 7$ and $a_0 = 0.25$, in all cases with $\eta = 4$.*

[1]Our formulation in this section is tailored to IA and hence it is only valid for $K > 1$. A slightly different approach would be required for $K = 1$.

A satisfactory agreement is observed in every case, supporting the validity of a complex Gaussian approximation for the out-of-cluster interference even if the information-theoretic arguments in support of a complex Gaussian interference model were ignored. Similar agreement has been observed for other values of the parameters.

C. Average Cluster Geometry

As the final step in the characterization of its distribution, we can average the instantaneous per-stream SIR over the ratio a_0.

Proposition 2. *Unconditioned on a_0,*

$$F_{\mathrm{SIR}}(\gamma) = 1 - \sum_{n=0}^{K-2} \frac{(-1)^n \, \Gamma(K)}{n! \, (K-2-n)! \, (n+1)} \cdot {}_2F_1\left(K, \frac{2(n+1)}{\eta}; 1 + \frac{2(n+1)}{\eta}; \frac{-2d\gamma}{\eta - 2}\right) \tag{21}$$

where ${}_2F_1(a, b; c; z)$ is the Gaussian hypergeometric function [30].

Proof: See Appendix C. ∎

Marginalized to the point that it depends only on the cluster size K and the number of signal streams d, the expression in Prop. 2 is less informative than the ones earlier in this section. In particular, it does not allow discriminating between situations that are either favorable or adverse to IA. And, as was the case for Prop. 1, it does not correspond to the distribution of the SIR experience by any actual user in the system, but rather it is a stepping stone towards the computation of average quantities. Moreover, its limited significance is buttressed by the fact that, barring an exclusion zone around the serving BS, the local-average SIR unconditioned on a_0 does not exist.

VI. Spectral Efficiency

The SIR improvements brought about by IA come at the expense of a sacrifice in the dimensionality of the transmit signal. Despite having N_t transmit and N_r receive antennas, only $d < \min(N_\mathrm{t}, N_\mathrm{r})$ parallel signals are conveyed and, therefore, to have a complete picture it is essential to look at the spectral efficiency, which is where the balance of signal dimensionality and SIR emerges. This section is devoted to characterizations of the spectral efficiency for each of the geometry marginalization scenarios put forth in Section V. Precisely, we characterize the ergodic spectral efficiency, which is the most operationally relevant quantity in contemporary systems where codewords span many fading realizations across frequency (because of the wide bandwidths), space (because of the multiplicity of antennas) and time (because of hybrid-ARQ) [31].

A. Specific Absolute Cluster Geometry

For a specific absolute cluster geometry we recover well-known expressions for Rayleigh fading [32], [33], only with the role of noise played by the out-of-cluster interference. For

$d = 1$, the ergodic spectral efficiency spawned by $F_{\mathrm{SIR}|\rho^{\mathsf{IA}}}(\cdot)$ in (18) is

$$\bar{C}^{\mathsf{IA}}_{\mathsf{abs}}(\rho^{\mathsf{IA}}) = \int_0^\infty \log_2(1+\gamma)\, \mathrm{d}F_{\mathrm{SIR}|\rho^{\mathsf{IA}}}(\gamma) \tag{22}$$

$$= e^{1/\rho^{\mathsf{IA}}} E_1\left(\frac{1}{\rho^{\mathsf{IA}}}\right) \log_2 e \tag{23}$$

where $E_n(\zeta) = \int_1^\infty t^{-n} e^{-\zeta t}\, \mathrm{d}t$ is an exponential integral and ρ^{IA} was given in (17). Through ρ^{IA}, the spectral efficiency depends on r_0 and r_{K-1}, as well as on the large-scale propagation parameters and the BS density.

For $d > 1$, (23) generalizes differently depending on whether the receiver applies separate per-stream decoding or joint decoding of the d streams. With separate per-stream decoding,

$$\bar{C}^{\mathsf{IA}}_{\mathsf{abs}}(\rho^{\mathsf{IA}}) = d\, e^{d/\rho^{\mathsf{IA}}} E_1\left(\frac{d}{\rho^{\mathsf{IA}}}\right) \log_2 e \tag{24}$$

while, recalling (7) and (16), under joint decoding

$$\bar{C}^{\mathsf{IA}}_{\mathsf{abs}}(\rho^{\mathsf{IA}}) = \mathbb{E}\left[\log_2 \det\left(\boldsymbol{I} + \frac{\rho^{\mathsf{IA}}}{d} \boldsymbol{W}_0^* \boldsymbol{H}_0 \boldsymbol{V}_0 \boldsymbol{V}_0^* \boldsymbol{H}_0^* \boldsymbol{W}_0\right) \,|\, \rho^{\mathsf{IA}}\right] \tag{25}$$

with expectation over the distribution of the effective fading $\boldsymbol{W}_0^* \boldsymbol{H}_0 \boldsymbol{V}_0 \in \mathbb{C}^{d\times d}$. Given the unitary nature of $\boldsymbol{V}_0$ and $\boldsymbol{W}_0$ and their independence from $\boldsymbol{H}_0$, we have that $\boldsymbol{W}_0^* \boldsymbol{H}_0 \boldsymbol{V}_0$ has IID entries drawn from $\mathcal{N}_{\mathbb{C}}(0,1)$. It follows that the right-hand-side of (25) is nothing but the ergodic spectral efficiency of a $d \times d$ Rayleigh-faded MIMO channel with IID entries and average signal-to-noise ρ^{IA}, under uniform power allocation, and thus

$$\bar{C}^{\mathsf{IA}}_{\mathsf{abs}}(\rho^{\mathsf{IA}}) = \bar{C}^{\mathsf{MIMO}}_{d,d}(\rho^{\mathsf{IA}}) \tag{26}$$

where the function [34]

$$\bar{C}^{\mathsf{MIMO}}_{N_{\mathrm{r}},N_{\mathrm{t}}}(\rho) = \log_2(e)\, e^{N_{\mathrm{t}}/\rho} \sum_{i=0}^{m-1} \sum_{j=0}^{i} \sum_{\ell=0}^{2j} \left[\binom{2i-2j}{i-j} \cdot \binom{2j+2n-2m}{2j-\ell} \frac{(-1)^\ell\, (2j)!\, (n-m+\ell)!}{2^{2i-\ell}\, j!\, \ell!\, (n-m+j)!} \cdot \sum_{q=0}^{n-m+\ell} E_{q+1}\left(\frac{N_{\mathrm{t}}}{\rho}\right)\right] \tag{27}$$

with $m = \min(N_{\mathrm{t}}, N_{\mathrm{r}})$ and $n = \max(N_{\mathrm{t}}, N_{\mathrm{r}})$ returns the ergodic capacity of a $N_{\mathrm{r}} \times N_{\mathrm{t}}$ Rayleigh-faded MIMO channel with IID entries and average signal-to-noise ρ.

B. Specific Relative Cluster Geometry

The spectral efficiency functionals in (24) and (26) depend, through ρ^{IA}, on both r_0 and r_{K-1} and they are thus fully general—in fact unnecessarily general for the purpose of assessing the benefits of IA. For that purpose, specifying the ratio a_0 is largely sufficient, as that allows marginalizing out the network dimensions while retaining the discrimination of relative in-cluster positions. Hence, we next seek a leaner characterization in the form of the average spectral efficiency over all possible cluster geometries that share a given a_0.

For arbitrary d under separate per-stream decoding, the marginalized ergodic spectral efficiency is

$$\bar{C}^{\mathsf{IA}}_{\mathsf{rel}}(a_0) = d\, \mathbb{E}\left[\mathbb{E}\left[\log_2(1+\mathrm{SIR})\,|\rho^{\mathsf{IA}}\right] \,|\, \tfrac{\mathsf{r}_0}{\mathsf{r}_{K-1}} = a_0\right] \tag{28}$$

$$= d\, \mathbb{E}\left[\log_2(1+\mathrm{SIR}) \,|\, \tfrac{\mathsf{r}_0}{\mathsf{r}_{K-1}} = a_0\right] \tag{29}$$

$$= d \int_0^\infty \log_2(1+\gamma)\, \mathrm{d}F_{\mathrm{SIR}|a_0}(\gamma) \tag{30}$$

and it is at this point that the conditional distribution $F_{\mathrm{SIR}|a_0}(\gamma)$ derived in Prop. 1 comes handy. Applying it to (30), the following result is obtained.

Proposition 3. *For a given a_0 under separate per-stream decoding,*

$$\bar{C}^{\mathsf{IA}}_{\mathsf{rel}}(a_0) = \frac{d \log_2 e}{K}\, {}_2F_1\left(1, K; K+1; 1 - \frac{2d\, a_0^\eta}{\eta - 2}\right) \tag{31}$$

Proof: See Appendix D. ∎

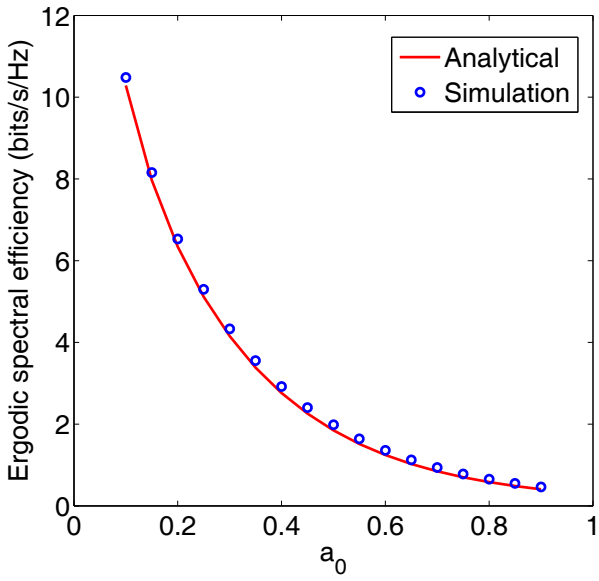

Fig. 2. Marginalized ergodic spectral efficiency of IA as function of a_0 for $K = 5$, $d = 1$ and $\eta = 4$.

Example 2. *Shown in Fig. 2 is a comparison, for $K = 5$, $d = 1$ and $\eta = 4$, of $\bar{C}^{\mathsf{IA}}_{\mathsf{rel}}(a_0)$ against its simulated counterpart with $\boldsymbol{z}'$ as in (3). The simulated result corresponds to the exact mutual information under the non-Gaussian interference in (3), computed through lengthy Monte-Carlo histograms and averaged over many fading realizations and out-of-cluster interference locations.*

In turn, for $d > 1$ under joint decoding,

$$\bar{C}^{\mathsf{IA}}_{\mathsf{rel}}(a_0) = \mathbb{E}\left[\bar{C}^{\mathsf{MIMO}}_{d,d}(\rho^{\mathsf{IA}}) \,|\, \tfrac{\mathsf{r}_0}{\mathsf{r}_{K-1}} = a_0\right] \tag{32}$$

where the expectation is over r_0 and r_{K-1}, conditioned on $\mathsf{r}_0/\mathsf{r}_{K-1} = a_0$. The right-hand side of (32) admits a closed form, given next.

Proposition 4. *For $d > 1$ and a given a_0, under joint decoding,*

$$\bar{C}^{\mathsf{IA}}_{\mathsf{rel}}(a_0) = \log_2(e) \sum_{i=0}^{d-1} \sum_{j=0}^{i} \sum_{\ell=0}^{2j} \frac{(-1)^\ell}{2^{2i-\ell}} \binom{2i-2j}{i-j} \binom{2j}{j} \binom{2j}{\ell} \cdot \sum_{m=0}^{\ell} \frac{1}{m+K} \, {}_2F_1\left(1, K; m+K+1; 1 - \frac{2d\, a_0^\eta}{\eta - 2}\right) \tag{33}$$

Proof: See Appendix E. ∎

C. Average Cluster Geometry

The spectral efficiencies in the previous section can be further expected over a_0 in order to characterize the average performance over all possible geometries. As was argued when the corresponding exercise was conducted for the SIR, this removes information on which the benefits of IA hinge, and hence what can be determined thereafter is only the average benefit of utilizing IA indiscriminately for all cluster geometries. At the same time, this computation evidences yet again the analytical muscle of stochastic geometry, yielding in compact form what in a deterministic model could only be attained through lengthy Monte-Carlo simulations.

For arbitrary d under separate per-stream decoding,

$$\bar{C}^{\mathsf{IA}} = d \int_0^\infty \log_2(1+\gamma) \, \mathrm{d}F_{\mathrm{SIR}}(\gamma) \tag{34}$$

where the unconditional SIR distribution $F_{\mathrm{SIR}}(\cdot)$ is given in (21). Remarkably, in that case the above expectation can be expressed by means of the Meijer-G function [35]

$$G^{m,n}_{p,q}\left(z \;\middle|\; \begin{matrix} a_1, \ldots, a_n, a_{n+1}, \ldots, a_p \\ b_1, \ldots, b_m, b_{m+1}, \ldots, b_q \end{matrix}\right) \tag{35}$$

which is readily available in software packages such as Mathematica or MATLAB.

Proposition 5. *Under separate per-stream decoding,*

$$\bar{C}^{\mathsf{IA}} = \frac{4d^2 \log_2 e}{\eta\,(\eta-2)} \sum_{n=0}^{K-2} \frac{(-1)^n}{n!\,(K-2-n)!} \cdot G^{2,3}_{3,3}\left(\frac{2d}{\eta-2} \;\middle|\; \begin{matrix} -1, -K, -\frac{2(n+1)}{\eta} \\ -1, -1, -\frac{\eta+2(n+1)}{\eta} \end{matrix}\right) \tag{36}$$

which, for $\eta = 4$, simplifies to

$$\bar{C}^{\mathsf{IA}} = \frac{d \log_2 e}{2^{K-1}} G^{2,4}_{4,4}\left(d \;\middle|\; \begin{matrix} 0, \frac{1}{2}, 0, 1-K \\ 0, 0, \frac{1-K}{2}, \frac{2-K}{2} \end{matrix}\right). \tag{37}$$

Proof: See Appendix F. ∎

For $d > 1$ under joint decoding, $\bar{C}^{\mathsf{IA}} = \mathbb{E}[\bar{C}^{\mathsf{MIMO}}_{d,d}(\rho^{\mathsf{IA}})]$ with expectation over r_0 and r_{K-1}, which ρ^{IA} is a function of.

Proposition 6. *Under joint decoding,*

$$\bar{C}^{\mathsf{IA}} = \frac{2\log_2 e}{\eta} \sum_{i=0}^{d-1} \sum_{j=0}^{i} \sum_{\ell=0}^{2j} \frac{(-1)^\ell}{2^{2i-\ell}} \binom{2i-2j}{i-j} \binom{2j}{j} \binom{2j}{\ell} \cdot \sum_{m=0}^{\ell} \frac{1}{m!} \left(\frac{2d}{\eta-2}\right)^{m+1} \sum_{n=0}^{K-2} \frac{(-1)^n}{n!\,(K-2-n)!} \cdot G^{2,3}_{3,3}\left(\frac{2d}{\eta-2} \;\middle|\; \begin{matrix} -(m+1), -(m+K), -\frac{m\eta+2(n+1)}{\eta} \\ -(m+1), -1, -\frac{\eta(m+1)+2(n+1)}{\eta} \end{matrix}\right) \tag{38}$$

Proof: See Appendix G. ∎

VII. System-level Benefits of IA

Having derived expressions for the ergodic spectral efficiency of IA, we can now put these expressions to work with the objective of ascertaining the system-level benefits of IA with respect to the SU-MIMO baseline.

A. SU-MIMO Baseline

As in IA, we consider a uniform power allocation for SU-MIMO, under which the ergodic spectral efficiency for a given absolute cluster geometry equals $\bar{C}^{\mathsf{MIMO}}_{N_{\mathrm{r}},N_{\mathrm{t}}}(\rho^{\mathsf{MIMO}})$ where the local-average SIR accounting for in-cluster and out-of-cluster interference, both present in SU-MIMO, is

$$\rho^{\mathsf{MIMO}} = \frac{\mathsf{r}_0^{-\eta}}{\sum_{k=1}^{K-1} \mathsf{r}_k^{-\eta} + \sigma_0^2} \tag{39}$$

$$= \frac{1}{\sum_{k=1}^{K-1} \left(\frac{a_0}{a_k}\right)^\eta + \frac{1}{\rho^{\mathsf{IA}}}} \tag{40}$$

where $a_k = \mathsf{r}_k / \mathsf{r}_{K-1}$.

The average spectral efficiency over all geometries sharing some common $a_0, \ldots, a_{K-1}$ equals

$$\mathbb{E}\left[\bar{C}^{\mathsf{MIMO}}_{N_{\mathrm{r}},N_{\mathrm{t}}}(\rho^{\mathsf{MIMO}}) \mid \tfrac{\mathsf{r}_k}{\mathsf{r}_{K-1}} = a_k\right] \tag{41}$$

with expectation over $\mathsf{r}_0, \ldots, \mathsf{r}_{K-1}$, which ρ^{MIMO} is function of, conditioned on $\mathsf{r}_k/\mathsf{r}_{K-1} = a_k$ for $k = 0, \ldots, K-1$.

Averaged over all cluster geometries, the SU-MIMO spectral efficiency is

$$\mathbb{E}\left[\bar{C}^{\mathsf{MIMO}}_{N_{\mathrm{r}},N_{\mathrm{t}}}(\rho^{\mathsf{MIMO}})\right] \tag{42}$$

with unconditional expectation over $\mathsf{r}_0, \ldots, \mathsf{r}_{K-1}$.

B. Benefits for Specific Cluster Geometries

We begin by establishing the benefits of IA for specific geometries, in order to identify the range of situations in which IA outperforms the SU-MIMO baseline. For this purpose, and in order to make assessments that do not rest on the absolute scale of the network, we apply the expressions derived for relative cluster geometries. We begin by equating

$$\bar{C}^{\mathsf{IA}}_{\mathsf{rel}}(\rho^{\mathsf{IA}}) = \mathbb{E}\left[\bar{C}^{\mathsf{MIMO}}_{N_{\mathrm{r}},N_{\mathrm{t}}}(\rho^{\mathsf{MIMO}}) \mid \tfrac{\mathsf{r}_k}{\mathsf{r}_{K-1}} = a_k\right] \tag{43}$$

and, utilizing the expressions derived for $\bar{C}^{\mathsf{IA}}_{\mathsf{rel}}(\cdot)$, ρ^{IA}, $\bar{C}^{\mathsf{MIMO}}_{N_{\mathrm{r}},N_{\mathrm{t}}}(\cdot)$ and ρ^{MIMO}, numerically determine the values for $a_0, \ldots, a_{K-1}$

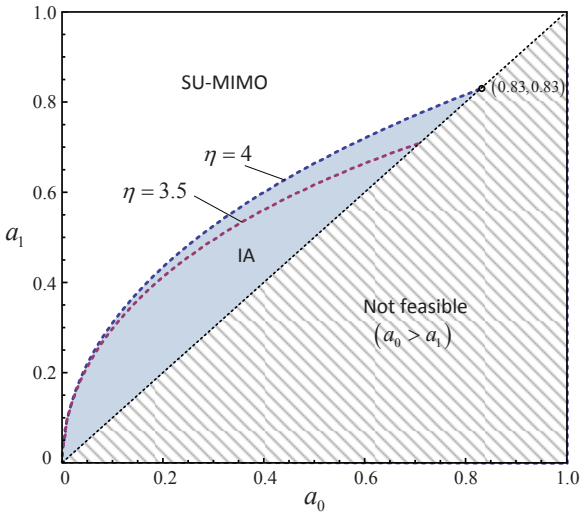

Fig. 3. IA (with $K = 3$ and $d = 1$) vs. SU-MIMO (with $N_{\rm t} = N_{\rm r} = 2$) for $\eta = 3.5$ and $\eta = 4$.

that define the boundary between the sets of geometries where IA and SU-MIMO are each superior.

Example 3. *Let $K = 3$ and $d = 1$, which can be supported with $N_{\rm t} = N_{\rm r} = 2$. Shown in Fig. 3 are the pairs (a_0, a_1) where IA and SU-MIMO are each superior for $\eta = 3.5$ and $\eta = 4$, which essentially delimit the range of pathloss exponents encountered in terrestrial systems. IA outperforms SU-MIMO in 20.5% and 26.7% of situations for $\eta = 3.5$ and $\eta = 4$, respectively.*

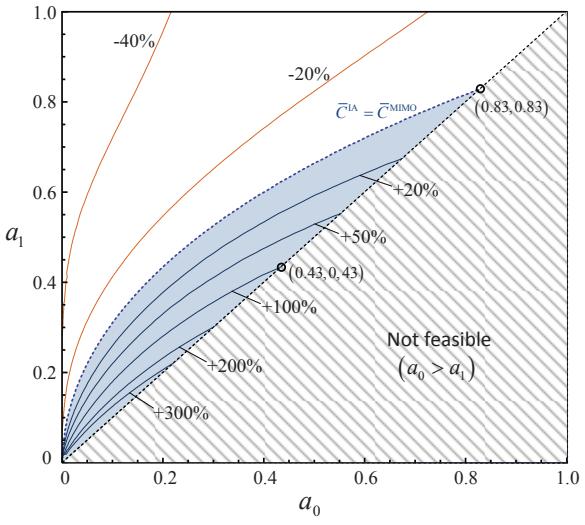

Fig. 4. Spectral efficiency gain of IA (with $K = 3$ and $d = 1$) over SU-MIMO (with $N_{\rm t} = N_{\rm r} = 2$), for $\eta = 4$.

Concentrating on $\eta = 4$, a more detailed snapshot of the comparison in Example 3 is offered in Fig. 4 where a contour plot of the relative improvement of IA over SU-MIMO is given. Notice that relatively important gains (say a doubling of the spectral efficiency) are attained in only a very small subset of geometries, specifically when a_0 is relatively small (weak out-of-cluster interference) and a_1 is similar to a_0 (strong in-cluster interference); only then does the removal of in-cluster interference compensate the sacrifice of signal dimensions.

To broaden the scope of the foregoing comparison, we next consider higher values of d and K along with the correspondingly higher values of $N_{\rm t}$ and $N_{\rm r}$.

Example 4 (Maintain K, increase d)**.** *Relative to Example 3 with $\eta = 4$, for $N_{\rm t} = N_{\rm r} = 4$ and $d = 2$ (with $K = 3$) the subset of geometries where IA outperforms SU-MIMO shrinks to 24.6% with joint decoding and to 15.3% with separate decoding.*

Example 5 (Maintain d, increase K)**.** *Relative to Example 3 with $\eta = 4$, for $N_{\rm t} = 2$, $N_{\rm r} = 3$ and $K = 4$ (with $d = 1$) the subset of geometries where IA outperforms SU-MIMO shrinks to 19.4%.*

Short of an exhaustive comparison for all combinations of d and K (and the corresponding $N_{\rm t}$ and $N_{\rm r}$), the above strongly suggest that IA can outperform the baseline in at most about a quarter of network geometries, often less.

Since the potential network geometries are not equally likely, a judgment based on average spectral efficiencies requires a further step.

C. Average Benefits

The small share of geometries in which IA outperforms the SU-MIMO baseline strongly suggests that, barring the possibility that those geometries occur very frequently, a blanket utilization of IA shall not improve the spatial averaged spectral efficiency over all geometries. To quantify this precisely, we can invoke the expressions derived for average cluster geometries. Shown in Table I we have a comparison of $\bar{C}^{\rm IA}$ and $\mathbb{E}\left[\bar{C}^{\rm MIMO}_{N_{\rm r},N_{\rm t}}(\rho^{\rm MIMO})\right]$ for several values of K and d, and corresponding values of $N_{\rm t}$ and $N_{\rm r}$, with $\eta = 4$. In every case, the average spectral efficiency of IA is inferior to that of SU-MIMO.

TABLE I
SPATIAL AVERAGED SPECTRAL EFFICIENCIES OF IA AND SU-MIMO FOR VARIOUS CLUSTER CONFIGURATIONS.

IA		SU-MIMO	
Configuration	(bits/s/Hz)	Configuration	(bits/s/Hz)
$K = 3$, $d = 1$	3.03	$N_{\rm t} = N_{\rm r} = 2$	3.89
$K = 3$, $d = 2$	5.84	$N_{\rm t} = N_{\rm r} = 4$	7.70
$K = 5$, $d = 1$	3.66	$N_{\rm t} = N_{\rm r} = 3$	5.76
$K = 5$, $d = 2$	7.06	$N_{\rm t} = N_{\rm r} = 6$	11.39
$K = 7$, $d = 1$	4.08	$N_{\rm t} = N_{\rm r} = 4$	7.70
$K = 7$, $d = 2$	7.87	$N_{\rm t} = N_{\rm r} = 8$	15.08

Although a blanket utilization of IA is not beneficial, there are situations (cf. Fig. 4) in which it is indeed advantageous. This points to a switched scheme that resorts to IA or SU-MIMO, whichever is best, depending on the geometry. From

the joint distribution of $a_0, \ldots, a_{K-1}$, the average gain of such a switched scheme can be quantified.

Example 6. *For $K = 3$, the average gain of a switched scheme relative to standalone SU-MIMO is 3.4% for $d = 1$ and 2.9% for $d = 2$.*

VIII. Conclusion

Leveraging the analytical potency of stochastic geometry and armed with a new modeling approach for out-of-cluster interference, we have derived analytical expressions for the ergodic spectral efficiency of IA. From these expressions, we observe that a universal utilization of IA in cellular networks would be ill-advised. IA can help in certain sets of BS and user locations—namely those resulting in strong in-cluster and weak out-of-cluster interference—and for users encountering such geometries the benefits can be substantial, but these geometries are relatively infrequent and the ensuing improvements in terms of average spectral efficiency for the system are rather minute.

The above observations have been made under assumptions highly favorable to IA and with a conservative baseline that does not even fully exploit the available CSI. With the degree of CSI required for IA, a superior MU-MIMO baseline could be implemented. Overheads associated with precoder computation [36], [37] have also been disregarded.

Non-unitary precoders and MMSE receivers would improve upon pure IA, but mostly in geometries where baseline schemes are already preferable.

Appendix A
Proof of (12)

Applying Campbell's theorem [38], [39] to expect over the location of all those out-of-cluster interferers whose distances exceed that of the farthest in-cluster BS r_{K-1}, we can express σ_0^2 as

$$\sigma_0^2 = 2\pi\lambda_{\mathsf{r}} \int_{\mathsf{r}_{K-1}}^{\infty} \mathsf{r}^{1-\eta}\, \mathrm{d}\mathsf{r} \tag{44}$$

from which (12) follows after solving the integral.

Appendix B
Proof of Proposition 1

To obtain the CDF, we need the density function of r_0 conditioned on $a_0 = \mathsf{r}_0/\mathsf{r}_{K-1}$, which can be obtained by using the joint density function of r_0 and r_{K-1}.

Lemma 1. *[40] Given a homogeneous PPP Φ_{r} of intensity λ_{r} with distances $\{\mathsf{r}_k\}$ satisfying $\mathsf{r}_0 < \mathsf{r}_1 < \ldots \mathsf{r}_{K-1}$, the joint PDF of r_0 and r_{K-1} is*

$$f_{\mathsf{r}_0,\mathsf{r}_{K-1}}(\mathsf{r}_0, \mathsf{r}_{K-1}) = \frac{4(\pi\lambda_{\mathsf{r}})^K \mathsf{r}_0 \mathsf{r}_{K-1}}{(K-2)!} \cdot e^{-\pi\lambda_{\mathsf{r}}\mathsf{r}_{K-1}^2} \left(\mathsf{r}_{K-1}^2 - \mathsf{r}_0^2\right)^{K-2}. \tag{45}$$

Utilizing $f_{\mathsf{r}_0,\mathsf{r}_{K-1}}(\cdot,\cdot)$, the joint PDF of r_0 and $a_0 = \mathsf{r}_0/\mathsf{r}_{K-1}$ can be computed as

$$f_{\mathsf{r}_0,a_0}(\mathsf{r}_0, a_0) = \frac{4(\pi\lambda_{\mathsf{r}})^K}{(K-2)!} e^{-\pi\lambda_{\mathsf{r}}(\mathsf{r}_0/a_0)^2} \left(\frac{\mathsf{r}_0}{a_0}\right)^3 \cdot \left(\left(\frac{\mathsf{r}_0}{a_0}\right)^2 - \mathsf{r}_0^2\right)^{K-2}. \tag{46}$$

Marginalizing this PDF over r_0 yields the PDF of a_0 as

$$f_{a_0}(a_0) = 2(K-1)\, a_0 \left(1 - a_0^2\right)^{K-2} \tag{47}$$

from which the PDF of r_0 conditioned on a_0 can be written as

$$f_{\mathsf{r}_0|a_0}(\mathsf{r}_0|a_0) = \frac{f_{\mathsf{r}_0,a_0}(\cdot,\cdot)}{f_{a_0}(\cdot)} \tag{48}$$

$$= \frac{2\left(\pi\lambda_{\mathsf{r}}\right)^K \mathsf{r}_0^{2K-1}}{\Gamma\left(K\right) a_0^{2K}} e^{-\pi\lambda_{\mathsf{r}}(\mathsf{r}_0/a_0)^2} \tag{49}$$

where $\Gamma(K) = \int_0^\infty e^{-t} t^{K-1}\, \mathrm{d}t$ is the Gamma function. Then, (19) is obtained by setting $\mathsf{r}_{K-1} = \mathsf{r}_0/a_0$ in (17) and averaging (18) over r_0 via the above conditional PDF.

Appendix C
Proof of Proposition 2

The expectation of (18) over r_0 and r_{K-1} via (45) yields

$$F_{\mathrm{SIR}}(\gamma) = 1 - \int_0^\infty \int_0^{\mathsf{r}_{K-1}} e^{-\gamma \frac{2\pi\lambda_{\mathsf{r}} d}{\eta-2} \frac{\mathsf{r}_0^\eta}{\mathsf{r}_{K-1}^{\eta-2}}} \frac{4(\pi\lambda_{\mathsf{r}})^K \mathsf{r}_0 \mathsf{r}_{K-1}}{(K-2)!} \cdot e^{-\pi\lambda_{\mathsf{r}}\mathsf{r}_{K-1}^2} \left(\mathsf{r}_{K-1}^2 - \mathsf{r}_0^2\right)^{K-2} \mathrm{d}\mathsf{r}_0\, \mathrm{d}\mathsf{r}_{K-1} \tag{50}$$

which, after applying the binomial expansion and solving the inner integral, becomes

$$F_{\mathrm{SIR}}(\gamma) = 1 - \sum_{n=0}^{K-2} \binom{K-2}{n} (-1)^n \frac{4(\pi\lambda_{\mathsf{r}})^K}{\eta\,(K-2)!} \alpha_1^{-\frac{2(n+1)}{\eta}} \cdot \int_0^\infty \frac{e^{-\pi\lambda_{\mathsf{r}}\mathsf{r}_{K-1}^2}}{\mathsf{r}_{K-1}^{-1-\nu}} \bar{\Gamma}\left(\frac{2(n+1)}{\eta}, \alpha_1 \mathsf{r}_{K-1}^2\right) \mathrm{d}\mathsf{r}_{K-1} \tag{51}$$

where $\alpha_1 = \frac{2d\gamma\pi\lambda_{\mathsf{r}}}{\eta-2}$ and

$$\nu = 2\left(K - 2 - n + \frac{(n+1)(\eta-2)}{\eta}\right) \tag{52}$$

while $\bar{\Gamma}(\cdot,\cdot)$ is the lower incomplete Gamma function. To solve the integral in (51), we effect the change of variable $\mathsf{r}_{K-1}^2 \to x$ and leverage [35, (6.455.2)] to obtain, after some algebra,

$$F_{\mathrm{SIR}}(\gamma) = 1 - \sum_{n=0}^{K-2} \frac{(-1)^n\,\Gamma(K)}{n!\,(K-2-n)!\,(n+1)} \left(1 + \alpha_2\,\gamma\right)^{-K} \cdot {}_2F_1\left(1, K; 1 + \frac{2(n+1)}{\eta}; \frac{\alpha_2\,\gamma}{1+\alpha_2\,\gamma}\right) \tag{53}$$

where $\alpha_2 = \frac{2d}{\eta-2}$. Finally, we use the transformation formula [35, (9.131.1)] to rewrite (53) in the more compact form claimed in (21).

APPENDIX D
PROOF OF PROPOSITION 3

The proofs of Props. 3 and 4 rest on the solution to

$$\mathcal{I}_1(m,y)=\int_0^\infty \frac{y^m\left(2^\gamma-1\right)^m}{\left(1+y\left(2^\gamma-1\right)\right)^{m+K}}\,\mathrm{d}\gamma \tag{54}$$

for any reals $m,y\geq 0$. Next, we provide an explicit solution to this integral.

Lemma 2. *For any reals $m,y\geq 0$,*

$$\mathcal{I}_1(m,y)=\log_2(e)\,\frac{\Gamma\left(K\right)\Gamma(m+1)}{\Gamma\left(K+m+1\right)} \cdot {}_2F_1(1,K;m+K+1;1-y). \tag{55}$$

Proof: With a simple change of variable and rescaling,

$$\mathcal{I}_1(m,y)=\frac{\log_2 e}{y^K}\int_0^\infty \frac{e^{-\gamma(K)}\left(1-e^{-\gamma}\right)^m}{\left(1+\frac{1-y}{y}e^{-\gamma}\right)^{m+K}}\,\mathrm{d}\gamma \tag{56}$$

which can be solved by virtue of [35, Eq. 3.312.3] giving

$$\mathcal{I}_1(m,y)=\frac{\log_2 e}{y^K}\,\frac{\Gamma\left(K\right)\Gamma(m+1)}{\Gamma\left(K+m+1\right)} \cdot {}_2F_1\left(m+K,K;m+K+1;1-\frac{1}{y}\right). \tag{57}$$

Transforming the hypergeometric function as per [35, Eq. 9.131.1], (57) reduces to (55). ∎

From (30), rewritten as

$$\bar{C}^{\mathsf{IA}}_{\mathsf{rel}}(a_0)=d\int_0^\infty \left(1-F_{\mathrm{SIR}|a_0}(2^\gamma-1)\right)\,\mathrm{d}\gamma \tag{58}$$

with $F_{\mathrm{SIR}|a_0}(\cdot)$ as given in (19),

$$\bar{C}^{\mathsf{IA}}_{\mathsf{rel}}(a_0)=d\int_0^\infty \left(1+\frac{2\,a_0^\eta\,d}{\eta-2}\left(2^\gamma-1\right)\right)^{-K}\mathrm{d}\gamma \tag{59}$$

$$=d\,\mathcal{I}_1\left(0,\frac{2\,a_0^\eta\,d}{\eta-2}\right) \tag{60}$$

and applying Lemma 2 with $m=0$ and $y=\frac{2a_0^\eta d}{\eta-2}$, we obtain the claimed expression in (31).

APPENDIX E
PROOF OF PROPOSITION 4

Recall that, under joint decoding, the spectral efficiency of IA is that of a $d\times d$ Rayleigh-faded MIMO channel with IID entries, which is computed via the marginal distribution of the eigenvalues of a Wishart matrix [34]. Thus,

$$\bar{C}^{\mathsf{IA}}_{\mathsf{rel}}(a_0)=d\int_0^\infty F^{\mathrm{c}}_{\mu|a_0}(2^\gamma-1)\,\mathrm{d}\gamma \tag{61}$$

where $F^{\mathrm{c}}_{\mu|a_0}(\cdot)$ is the complementary CDF, conditioned on a_0, of the (unordered) eigenvalues of the Wishart matrix

$$\boldsymbol{Y}=\frac{\rho^{\mathsf{IA}}}{d}\boldsymbol{W}_0^*\boldsymbol{H}_0\boldsymbol{V}_0\boldsymbol{V}_0^*\boldsymbol{H}_0^*\boldsymbol{W}_0. \tag{62}$$

From [34, Eq. 42], the complementary CDF of an (unordered) eigenvalue conditioned on ρ^{IA} equals

$$F^{\mathrm{c}}_{\mu|\rho^{\mathsf{IA}}}(x)=\frac{1}{d}\sum_{i=0}^{d-1}\sum_{j=0}^{i}\sum_{\ell=0}^{2j}\frac{(-1)^\ell}{2^{2i-\ell}\ell!}\binom{2i-2j}{i-j}\binom{2j}{j}\binom{2j}{\ell} \cdot\Gamma\left(\ell+1,\frac{d}{\rho^{\mathsf{IA}}}x\right). \tag{63}$$

To obtain $F^{\mathrm{c}}_{\mu|a_0}(\cdot)$, we set $\rho^{\mathsf{IA}}=\frac{\mathsf{r}_{K-1}^{\eta-2}}{\mathsf{r}_0^\eta}\frac{\eta-2}{2\pi\lambda_{\mathsf{r}}}$ and $\mathsf{r}_{K-1}=\mathsf{r}_0/a_0$ in (63) and expect over conditional density (49) obtaining

$$F^{\mathrm{c}}_{\mu|a_0}(x)=\frac{1}{d}\sum_{i=0}^{d-1}\sum_{j=0}^{i}\sum_{\ell=0}^{2j}\frac{(-1)^\ell}{2^{2i-\ell}\ell!}\binom{2i-2j}{i-j}\binom{2j}{j}\binom{2j}{\ell}\mathcal{J}(x) \tag{64}$$

where

$$\mathcal{J}(x)=\int_0^\infty\Gamma\left(\ell+1,\frac{2\pi\lambda_{\mathsf{r}}a_0^{\eta-2}\mathsf{r}_0^2 d}{\eta-2}x\right)\frac{2\left(\pi\lambda_{\mathsf{r}}\right)^K\mathsf{r}_0^{2K-1}}{\Gamma\left(K\right)a_0^{2K}} \cdot e^{-\pi\lambda_{\mathsf{r}}(\mathsf{r}_0/a_0)^2}\mathrm{d}\mathsf{r}_0$$

$$=\ell!\sum_{m=0}^{\ell}\frac{1}{m!}\frac{\Gamma\left(m+K\right)}{\Gamma\left(K\right)}\frac{\left(\frac{2a_0^\eta d}{\eta-2}x\right)^m}{\left(1+\frac{2a_0^\eta d}{\eta-2}x\right)^{m+K}} \tag{65}$$

where (65) follows from the expansion of the incomplete Gamma function [35, Eq. 8.352.2], which allows solving the integral with the change of variable $\mathsf{r}_0^2\to\mathsf{r}'$.

Combining (64) and (65) and plugging the resulting expression for $F^{\mathrm{c}}_{\mu|a_0}(\cdot)$ in (61), we arrive at

$$\bar{C}^{\mathsf{IA}}_{\mathsf{rel}}(a_0)=\sum_{i=0}^{d-1}\sum_{j=0}^{i}\sum_{\ell=0}^{2j}\frac{(-1)^\ell}{2^{2i-\ell}}\binom{2i-2j}{i-j}\binom{2j}{j}\binom{2j}{\ell} \cdot\sum_{m=0}^{\ell}\frac{1}{m!}\frac{\Gamma\left(m+K\right)}{\Gamma\left(K\right)}\,\mathcal{I}_1\left(m,\frac{2\,a_0^\eta\,d}{\eta-2}\right) \tag{66}$$

where $\mathcal{I}_1(\cdot,\cdot)$ is the integral in Lemma 2, from which (33) follows after further simplifications.

APPENDIX F
PROOF OF PROPOSITION 5

The proofs of Props. 5 and 6 rest on the solution to

$$\mathcal{I}_2(m,n,y)=\int_0^\infty y^m\left(2^\gamma-1\right)^m \cdot {}_2F_1(K+m,m+\eta';m+1+\eta';-y(2^\gamma-1))\,\mathrm{d}\gamma \tag{67}$$

for any reals $m,y\geq 0$ and $\eta'=\frac{2(n+1)}{\eta}$ with real $n\geq 0$. Next, we provide an explicit solution to this integral.

Lemma 3. *For any reals $m,y\geq 0$,*

$$\mathcal{I}_2(m,n,y)=\log_2(e)\,y^{m+1}\frac{m+\eta'}{\Gamma(K+m)} \cdot G^{2,3}_{3,3}\left(y\,\middle|\,\begin{matrix}-(m+1),-(m+K),-m-\eta'\\-(m+1),-1,-m-1-\eta'\end{matrix}\right) \tag{68}$$

Proof: The change of variable $(2^\gamma - 1) \to x$ in (67) yields

$$\mathcal{I}_2(m,n,y) = \log_2(e)\, y^m \int_0^\infty \frac{x^m}{1+x} \cdot {}_2F_1(K+m, m+\eta'; m+1+\eta'; -y\,x)\, \mathrm{d}x. \tag{69}$$

By virtue of [35, Eq. 9.34.7], the hypergeometric function in (69) can be expressed in terms of the Meijer-G function and the resulting integral has the explicit solution in (68) according to [35, Eq. 7.811.5]. ∎

The spectral efficiency is computed as

$$\bar{C}^{\mathsf{IA}} = d \int_0^\infty (1 - F_{\mathrm{SIR}}(2^\gamma - 1))\, \mathrm{d}\gamma \tag{70}$$

with $F_{\mathrm{SIR}}(\cdot)$ as given in (21). Plugging (21) into (70),

$$\bar{C}^{\mathsf{IA}} = d \sum_{n=0}^{K-2} \frac{(-1)^n\, \Gamma(K)}{n!\,(K-2-n)!\,(n+1)}\, \mathcal{I}_2\left(0, n, \frac{2d}{\eta - 2}\right) \tag{71}$$

where $\mathcal{I}_2(m,n,y)$ was given in Lemma 3, from which (36) follows after replacing $\eta' \to \frac{2(n+1)}{\eta}$ and simplifying.

Appendix G
Proof of Proposition 6

This proof follows an approach similar to the one in Appendix E and some details are thus omitted for brevity. Here, we need to obtain $F_\mu^{\mathrm{c}}(\cdot)$, the complementary CDF of the eigenvalues of $\boldsymbol{Y}$ averaged over all possible cluster geometries. To that end, we average $F_{\mu|\rho^{\mathsf{IA}}}^{\mathrm{c}}(\cdot)$ in (63) over r_0 and r_{K-1} via its joint density, given in (45), arriving at

$$F_\mu^{\mathrm{c}}(x) = \frac{1}{d} \sum_{i=0}^{d-1} \sum_{j=0}^{i} \sum_{\ell=0}^{2j} \frac{(-1)^\ell}{2^{2i-\ell}\ell!} \binom{2i-2j}{i-j} \binom{2j}{j} \binom{2j}{\ell} \mathcal{K}(x) \tag{72}$$

where

$$\mathcal{K}(x) = \int_0^\infty \int_0^{\mathsf{r}_{K-1}} \Gamma\left(\ell + 1, \frac{2\pi\lambda_{\mathsf{r}} d}{\eta - 2} \frac{\mathsf{r}_0^\eta}{\mathsf{r}_{K-1}^{\eta-2}} x\right) \frac{4(\pi\lambda_{\mathsf{r}})^K}{(K-2)!} \cdot e^{-\pi\lambda_{\mathsf{r}}\mathsf{r}_{K-1}^2} \mathsf{r}_0 \mathsf{r}_{K-1} \left(\mathsf{r}_{K-1}^2 - \mathsf{r}_0^2\right)^{K-2} \mathrm{d}\mathsf{r}_0\, \mathrm{d}\mathsf{r}_{K-1}. \tag{73}$$

Expanding the incomplete Gamma function as in [35, Eq. 8.352.2], (73) turns into a sum where each term is a double integral of the same type that (50), solved in Appendix C. The same steps are followed here, yielding

$$\mathcal{K}(x) = \frac{2\,\ell!}{\eta} \sum_{m=0}^{\ell} \frac{1}{m!} \sum_{n=0}^{K-2} \frac{(-1)^n \Gamma(K+m)}{n!\,(K-2-n)!\,(m+\eta')} \cdot \left(\frac{2d}{\eta-2} x\right)^m {}_2F_1\left(K+m, m+\eta'; m+1+\eta'; \frac{-2d}{\eta-2} x\right) \tag{74}$$

where $\eta' = \frac{2(n+1)}{\eta}$.

Combining (72) and (74) and integrating the result as

$$\bar{C}^{\mathsf{IA}} = d \int_0^\infty F_\mu^{\mathrm{c}}(2^\gamma - 1)\, \mathrm{d}\gamma \tag{75}$$

yields the spectral efficiency

$$\bar{C}^{\mathsf{IA}} = \frac{2}{\eta} \sum_{i=0}^{d-1} \sum_{j=0}^{i} \sum_{\ell=0}^{2j} \frac{(-1)^\ell}{2^{2i-\ell}} \binom{2i-2j}{i-j} \binom{2j}{j} \binom{2j}{\ell} \cdot \sum_{m=0}^{\ell} \frac{1}{m!} \sum_{n=0}^{K-2} \frac{(-1)^n \Gamma(K+m)}{n!\,(K-2-n)!\,(m+\eta')}\, \mathcal{I}_2\left(m, n, \frac{2d}{\eta-2}\right) \tag{76}$$

where $\mathcal{I}_2(m,n,y)$ was given in Lemma 3, from which (38) follows after replacing $\eta' \to 2(n+1)/\eta$ and simplifying.

Acknowledgments

The excellent feedback provided by the reviewers is gratefully acknowledged.

References

[1] R. K. Mungara, D. Morales-Jimenez, and A. Lozano, "System-level performance of interference alignment," IEEE GLOBECOM'14, 2014.

[2] K. Gomadam, V. Cadambe, and S. Jafar, "A distributed numerical approach to interference alignment and applications to wireless interference networks," *IEEE Trans. Inform. Theory*, vol. 57, no. 6, pp. 3309–3322, June 2011.

[3] S. W. Peters and R. W. Heath Jr., "Interference alignment via alternating minimization," in *Proc. IEEE Int. Conf. Acoust., Speech, Signal Processing*, Apr. 2009, pp. 2445–2448.

[4] V. Cadambe and S. A. Jafar, "Interference alignment and the degrees of freedom of the K-user interference channel," *IEEE Trans. Inform. Theory*, vol. 54, no. 8, pp. 3425–3441, Aug. 2008.

[5] M. Maddah-Ali, A. Motahari, and A. Khandani, "Communication over MIMO X channels: Interference alignment, decomposition, and performance analysis," *IEEE Trans. Inform. Theory*, vol. 54, no. 8, pp. 3457–3470, Aug. 2008.

[6] A. Lozano, R. W. Heath Jr., and J. G. Andrews, "Fundamental limits of cooperation," *IEEE Trans. Inform. Theory*, vol. 59, no. 9, pp. 5213–5226, Sept. 2013.

[7] C. Suh and D. Tse, "Interference alignment for cellular networks," in *Proc. Annual Allerton Conf. Commun., Cont., Computing*, Sept. 2008, pp. 1037–1044.

[8] C. Suh, M. Ho, and D. Tse, "Downlink interference alignment," *IEEE Trans. Commun.*, vol. 59, no. 9, pp. 2616–2626, Sept. 2011.

[9] R. Mungara, G. George, and A. Lozano, "System-level performance of distributed cooperation," in *Proc. Annual Asilomar Conf. Signals, Syst., Comp.*, Nov. 2012.

[10] D. Aziz, F. Boccardi, and A. Weber, "System-level performance study of interference alignment in cellular systems with base-station coordination," in *Proc. IEEE Int. Symp. Pers., Indoor, Mobile Radio Commun.*, Sydney, Australia, Sept. 2012, pp. 1177–1182.

[11] M. Z. Win, P. C. Pinto, and L. A. Shepp, "A mathematical theory of network interference and its applications," *Proc. IEEE*, vol. 97, no. 2, pp. 205–230, Feb. 2009.

[12] J. G. Andrews, F. Baccelli, and R. K. Ganti, "A tractable approach to coverage and rate in cellular networks," *IEEE Trans. Commun.*, vol. 59, no. 11, pp. 3122–3134, Nov. 2011.

[13] H. S. Dhillon, R. K. Ganti, F. Baccelli, and J. G. Andrews, "Modeling and analysis of k-tier downlink heterogeneous cellular networks," *IEEE J. Select. Areas Commun.*, vol. 30, no. 3, pp. 550–560, Apr. 2012.

[14] S. Mukherjee, "Distribution of downlink SINR in heterogeneous cellular networks," *IEEE J. Select. Areas Commun.*, vol. 30, no. 3, pp. 575–585, Apr. 2012.

[15] K. Huang and J. G. Andrews, "An analytical framework for multicell cooperation via stochastic geometry and large deviations," *IEEE Trans. Inform. Theory*, vol. 59, no. 4, pp. 2501–2516, Apr. 2013.

[16] S. Akoum and R. W. Heath Jr., "Interference coordination: random clustering and adaptive limited feedback," *IEEE Trans. Signal Processing*, vol. 61, no. 7, pp. 1822–1834, Apr. 2013.

[17] N. Lee, D. Morales-Jimenez, A. Lozano, and R. W. Heath Jr., "Spectral efficiency of dynamic coordinated beamforming: A stochastic geometry approach," *IEEE Trans. Wireless Commun., to appear*, 2014.

[18] A. Guo and M. Haenggi, "Spatial stochastic models and metrics for the structure of base stations in cellular networks," *IEEE Trans. Wireless Commun.*, vol. 12, no. 11, pp. 5800–5812, 2013.
[19] N. Deng, W. Zhou, and M. Haenggi, "The Ginibre point process as a model for wireless networks with repulsion," *IEEE Trans. Wireless Commun., submitted*, 2014.
[20] A. Papadogiannis, D. Gesbert, and E. Hardouin, "A dynamic clustering approach in wireless networks with multi-cell cooperative processing," in *Proc. IEEE Int. Conf. Commun.*, May 2008, pp. 4033–4037.
[21] H. Wang and M. C. Reed, "Tractable model for heterogeneous cellular networks with directional antennas," in *Proc. Australian Commun. Theory Workshop*, Wellington, New Zeland, Jan. 2012, pp. 61–65.
[22] J. Wildman, P. H. J. Nardelli, S. Weber, and M. Latva-aho, "On the joint impact of beamwidth and orientation error on throughput in wireless directional poisson networks," Available online: http://arxiv.org/abs/1312.6057, 2013.
[23] P. Madhusudhanan, J. G. Restrepo, Y. E. Liu, and T. X. Brown, "Carrier to Interference ratio analysis for the shotgun cellular system," in *Proc. IEEE Global Telecommun. Conf.*, Honolulu, USA, Nov. 2009, pp. 1–6.
[24] L. Ruan, V. K. N. Lau, and M. Z. Win, "The feasibility conditions for interference alignment in MIMO networks," *IEEE Trans. Signal Processing*, vol. 61, no. 8, pp. 2066–2077, Nov. 2013.
[25] K. Gulati, B. L. Evans, J. G. Andrews, and K. R. Tinsley, "Statistics of co-channel interference in a field of Poisson and Poisson-Poisson clustered interferers," *IEEE Trans. Signal Processing*, vol. 58, no. 12, pp. 6207–6222, Dec. 2010.
[26] B. Nosrat-Makouei, J. G. Andrews, R. W. Heath Jr., and R. K. Ganti, "MIMO interference alignment in random access networks," in *Proc. Annual Asilomar Conf. Signals, Syst., Comp.*, Nov. 2011, pp. 641–645.
[27] N. Pappas and M. Kountouris, "Performance analysis of distributed cooperation under uncoordinated network interference," in *Proc. IEEE Int. Conf. Acoust., Speech, Signal Processing*, May 2014.
[28] M. Di Renzo and P. Guan, "A mathematical framework to the computation of the error probability of downlink mimo cellular networks by using stochastic geometry," *IEEE Trans. Commun.*, vol. 62, no. 8, pp. 2860–2879, Aug. 2014.
[29] A. Lapidoth and S. Shamai, "Fading channels: how perfect need "perfect side information" be?," *IEEE Trans. on Inform. Theory*, vol. 48, no. 5, pp. 1118–1134, 2002.
[30] F. Beukers, "Gauss' hypergeometric function," in *Arithmetic and geometry around hypergeometric functions*, vol. 260 of *Progress in Mathematics*, pp. 23–42. Birkhäuser Verlag Basel, Switzerland, 2007.
[31] A. Lozano and N. Jindal, "Are yesterday's information-theoretic fading models and performance metrics adequate for the analysis of today's wireless systems?," *IEEE Commun. Mag.*, vol. 50, no. 11, pp. 210–217, Nov. 2012.
[32] W. C. Y. Lee, "Estimate of channel capacity in Rayleigh fading environments," *IEEE Trans. Veh. Technol.*, vol. 39, no. 3, pp. 187–189, Aug. 1990.
[33] L. Ozarow, S. Shamai, and A. D. Wyner, "Information theoretic considerations for cellular mobile radio," *IEEE Trans. Veh. Technol.*, vol. 43, no. 2, pp. 359–378, May 1994.
[34] H. Shin and J. H. Lee, "Capacity of multiple-antenna fading channels: spatial fading correlation, double scattering, and keyhole," *IEEE Trans. Inform. Theory*, vol. 49, no. 10, pp. 2636–2647, Oct. 2003.
[35] I. S. Gradshteyn and I. M. Ryzhik, *Table of Integrals, Series, and Products*, Academic Press, San Diego, 7th edition, 2007.
[36] R. K. Mungara, G. George, and A. Lozano, "Overhead and spectral efficiency of pilot-assisted interference alignment in time-selective fading channels," *IEEE Trans. Wireless Commun., to appear*, 2014.
[37] O. El Ayach, A. Lozano, and R. W. Heath Jr., "On the overhead of interference alignment: Training, feedback, and cooperation," *IEEE Trans. on Wireless Communications*, vol. 11, no. 11, pp. 4192–4203, 2012.
[38] D. Stoyan, W. S. Kendall, and J. Mecke, *Stochastic Geometry and its Applications*, John Wiley & Sons Ltd, New York, USA, 2nd edition, 1995.
[39] M. Haenggi, *Stochastic Geometry for Wireless Networks*, Cambridge Univ. Press, Cambridge, U. K., 2012.
[40] D. Moltchanov, "Distance distributions in random networks," *Ad Hoc Networks*, vol. 10, no. 6, pp. 1146–1166, Aug. 2012.

Ratheesh K. Mungara received the B.Tech. degree in Electronics and Communications Engineering from Jawaharlal Nehru Technological University, Hyderabad, India, in 2005, and the M.Tech. degree in Communication Systems from the National Institute of Technology, Tiruchirappalli, India, in 2007.

He is currently working toward his Ph.D. with the Wireless Communications research group, Department of Information and Communication Technologies, UPF (Universitat Pompeu Fabra), Barcelona, Spain. He was an engineer at Qualcomm India Private Limited, Hyderabad, from 2007-2010, and a research scientist at the Centre for Wireless Communications (CWC), University of Oulu, Finland, during 2010-2011. His general research interests are modeling and analysis of wireless networks using stochastic geometry tools. His current focus is on interference management techniques and Device-to-Device communication.

David Morales-Jimenez received the Telecommunication Engineering degree from the University of Málaga (Spain) in 2006, and the M.S. and Ph.D. degrees in Telecommunication Technologies from the same University in 2008 and 2011, respectively. Between 2011 and 2013 he worked in the Wireless Communications Research Group (WiCom), headed by Prof. Angel Lozano at the Department of Information and Communication Technologies, Universitat Pompeu Fabra, Barcelona (Spain), where he was a post-doctoral fellow and a lecturer. In January 2014, he joined the research group of Prof. Matthew McKay at the Department of Electronic and Computer Engineering, Hong Kong University of Science and Technology (HKUST), where he holds a Visiting Scholar position.

His research activity lies between the communication theory and signal processing areas, with a focus on wireless communications. His current research interests include: spectrum sharing, interference characterization through stochastic geometry tools, and massive MIMO. He is a recipient of the best PhD Thesis Award in Electrical and Computer Engineering by the University of Malaga (selected among all PhD Theses between 2009-2012).

Angel Lozano is a Professor of Information and Communication Technologies at UPF (Universitat Pompeu Fabra) in Barcelona, Spain. He received the MSc. and Ph.D. degrees in Electrical Engineering from Stanford University in 1994 and 1998, respectively. In 1999 he joined Bell Labs (Lucent Technologies, now Alcatel-Lucent) in Holmdel, USA, where he was a member of the Wireless Communications Research Department until 2008. Between 2005 and 2008 he was also Adj. Associate Professor of Electrical Engineering at Columbia University.

Prof. Lozano is a Fellow of the IEEE since 2014. He is an associate editor for the IEEE Transactions on Information Theory (since 2011), a former editor for the IEEE Transactions on Communications (1999-2009) and the Journal of Communications & Networks (2010-2012), has guest-edited various journal special issues, and is actively involved in committees and conference organization tasks for the IEEE. In particular, he is the Chair of the IEEE Communication Theory Technical Committee (2013-2014) and was elected to the Board of Governors of the IEEE Communications Society (2012-2014). He has further participated in standardization activities for 3GPP, 3GPP2, IEEE 802.20 and the IETF.

Prof. Lozano has published extensively, holds 15 patents, and has contributed to several books. His papers have received two awards: the best paper at the 2006 IEEE Int'l Symposium on Spread Spectrum Techniques & Applications, and the Stephen O. Rice prize to the best paper published in the IEEE Transactions on Communications in 2008. He also received the Bell Labs President's Gold Award in 2002 and the ICREA Academia Award